

DIAGNOSTIC NUCLEAR MEDICINE

Measurements of Regional Tissue and Blood-Pool Radiotracer Concentrations from Serial Tomographic Images of the Heart

Eberhard Henze, Sung-Cheng Huang, Osman Ratib*, Edward Hoffman, Michael E. Phelps, and Heinrich R. Schelbert

UCLA School of Medicine, and University of California at Los Angeles, Los Angeles, California

Quantification of myocardial tissue kinetics from serial tomographic images is limited because of bidirectional cross-contamination of recorded counts between myocardium and blood for metabolic tracers with relative slow blood clearance. We have developed and validated a new deconvolution technique that permits calculation of spillover fractions derived from geometric measurements of the imaged cross section (wall thickness, chamber diameter) and the intrinsic resolution of the tomograph. Serial gated positron-emission computerized imaging (PCT) and a-v blood sampling across the heart were performed in five dogs for 45 min after i.v. C-11 palmitate (CPA) and in five dogs for 3 hr after i.v. F-18 deoxyglucose (FDG). Tracer concentrations in myocardial tissue and arterial blood were also measured in vitro. Uncorrected PCT tissue and blood concentrations correlated poorly with in vitro measurements. After correction for count crossover, the correlation for FDG in tissue was $r = 0.99$, for FDG in blood $r = 0.97$, and for CPA in blood $r = 0.99$. Deconvolution techniques applied to serial PCT images provide accurate noninvasive measurement of myocardial tracer concentrations and direct determination of the arterial input function required for measurements of myocardial metabolism.

J Nucl Med 24: 987-996, 1983

With the recent development of emission imaging devices for positron or single photon tomographic display of the local tracer distribution in organs in vivo (1-3), and the availability of numerous labeled substrates (4,5), the noninvasive study of myocardial metabolism has become possible. Tracers to monitor metabolism of free fatty acid (4-7), glucose (4,5,8-10), and amino acids (11-13) have been labeled with positron emitters for positron-emission computerized tomography (PCT), and iodine- (14-16) or tellurium-labeled (17) fatty acid analogs have been used in connection with conventional gamma cameras or single photon computerized to-

mography (SPECT). However, most tomographic studies performed to date have evaluated the myocardial uptake of metabolic tracers only qualitatively or semi-quantitatively—for example to determine the size of a myocardial infarct with C-11 palmitate and PCT (18,19).

For measurements of regional metabolic processes such as uptake and turnover rates of substrates, quantitative determinations of tracer concentrations and their rates of change are needed. Positron CT offers the potential capability of noninvasive measurement of tissue tracer concentrations (1-3). This capability is somewhat limited in the heart because of the relative low spatial resolution of only 10 to 20 mm, full-width at half-maximum, of most existing imaging devices (1-3). This relatively low resolution causes an underestimation of the true myocardial tissue activity due to the partial-volume effect (20) and a considerable bidirectional ac-

Received Nov. 17, 1982; revision accepted May 3, 1983.

For reprints contact: Heinrich R. Schelbert, MD, Division of Nuclear Medicine, UCLA School of Medicine, Los Angeles, CA 90024.

* Present address: Dept. of Cardiology, Hospital Cantonal, University of Geneva, Geneva, Switzerland.

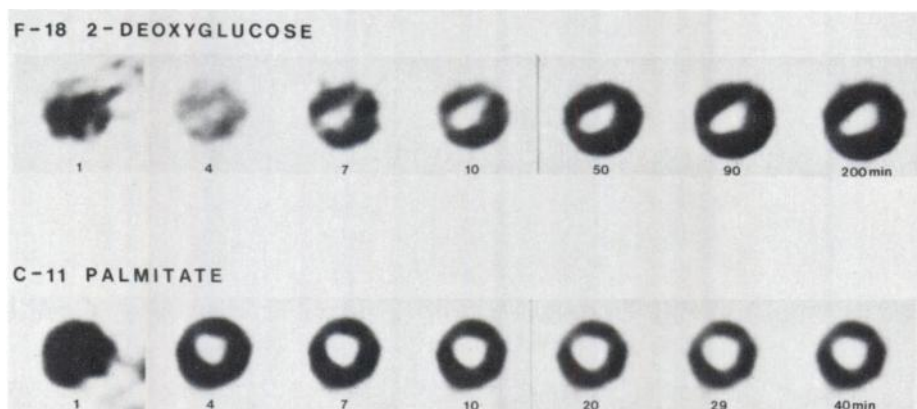


FIG. 1. Serial gated myocardial PCT images obtained perpendicular to long axis of dog's left ventricle after i.v. injection of F-18 deoxyglucose (upper panel) or C-11 palmitate (lower panel). Note that after F-18 deoxyglucose injection there is continuous accumulation of activity, whereas C-11 palmitate activity shows initial high uptake followed by washout phase.

tivity cross-contamination between blood pools and myocardial tissue on the tomographic images (21). While limitations related to the partial-volume effect can be overcome by measuring myocardial wall thickness and the use of a correction factor, as reported from our laboratory (20,22), cross-contamination of counts causes a more serious problem, in particular with sequential imaging for tracer kinetic studies with metabolic tracers that are cleared relatively slowly from blood pool—such as F-18 deoxyglucose (F-18 DG), or C-11 palmitate (C-11 PA), or amino acids labeled with N-13 or C-11. Persistent blood activity will contaminate the early, (usually important) portion of the tissue time-activity curves by spillover of counts from the blood-pool region into the myocardial regions on the images. Conversely, on the late tomographic images (when tracer blood pool activity is low but myocardial tissue activity is high), blood-pool activity will be overestimated due to spillover of the high tissue count rate. Although the large blood pools adjacent to the myocardium adversely affect quantitative retrieval of tissue activity from tomographic images of the heart, they offer the possibility of measuring noninvasively blood-pool tracer kinetics together with myocardial tissue concentrations from serial tomograms. Knowledge of blood-pool time-activity kinetics is required for determining the tracer input function when metabolic rate constants are to be calculated using tracer kinetic models (23,24).

It was thus the purpose of this study (a) to develop a mathematical deconvolution technique for accurate retrieval of activity concentrations in both myocardial tissue and the arterial blood pool from serial tomographic images; and (b) to validate this technique in animal experiments with PCT and two tracers of myocardial metabolism, F-18 DG and C-11 PA.

METHODS

Theoretical considerations. The problem encountered

with measuring regional indicator tissue concentrations by PCT after intravenous injection of C-11 PA or F-18 DG is illustrated in Fig. 1. The activity is present primarily in the blood pools on the first image acquired at 1 min. It is subsequently cleared slowly from blood while myocardial F-18 activity increases with time, whereas C-11 activity slowly declines in myocardium after reaching an early peak. In both studies there is a time when tracer concentrations in blood are high and there is significant spillover of counts into myocardium. Conversely, there is a time when tracer concentrations are low in blood and high in myocardium and there is spillover of counts from myocardium into the left-ventricular (LV) chamber. Therefore, counts derived from regions of interest assigned to the LV myocardium or the LV blood pool are contaminated by spillover of counts from myocardium and blood. These limitations are further illustrated in Fig. 2, which shows two PCT images of a dog's heart. One image was obtained after O-15 CO inhalation to label only the blood pool, and the other after injection of Ga-68 microspheres into the left atrium to label only myocardium. These images illustrate the effects of cross-contamination of counts and the partial-volume effect. The effects can be corrected by the operational equations shown in the Appendix, assuming that the imaging resolution and the geometric dimensions of the heart's cross section are known. These equations are also shown in Fig. 2 and their derivation is in the Appendix.

Animal preparation. Ten mongrel dogs weighing 20–30 kg were anesthetized with sodium pentobarbital (25 mg/kg, i.v.), intubated, and ventilated with room air from a Harvard respirator. Catheters were advanced through both femoral arteries into the aorta for monitoring systemic blood pressure and withdrawal of arterial blood for measurements of myocardial blood flow with radioactive microspheres (25). After a left thoracotomy, the pericardium was incised widely and sutured to the chest wall to form a cradle suspending the heart. Two

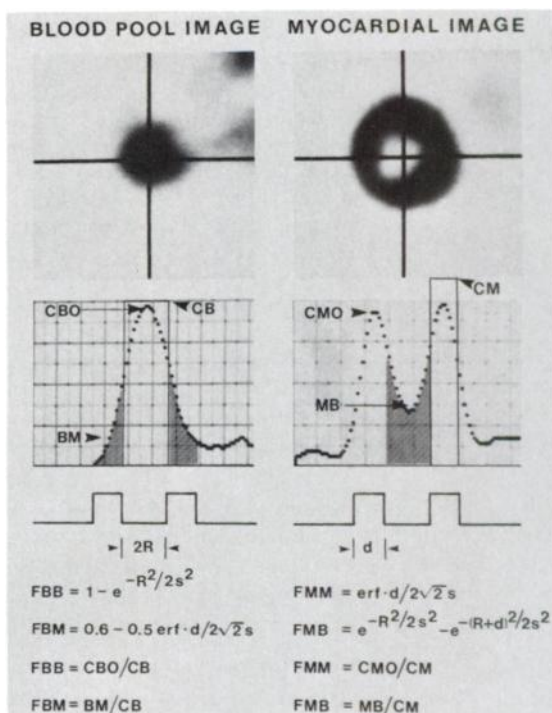


FIG. 2. Histograms (lower panel) from PCT blood-pool (upper left) and myocardial (upper right) images. Blood pool was labeled with ^{11}C O; myocardium with Ga-68 albumin microspheres. Histograms are roughly Gaussian, with measureable cross-contamination of blood-pool counts into myocardial areas (BM) or from myocardial to blood-pool areas (MB). Fractional spillover (FBM or FMB) can be calculated from observed activities (CBO, CMO), from measured diameter ($2R$), wall thickness (d), and spatial resolution of imaging system (s). FBB and FMM indicate recovery coefficient necessary to correct for partial-volume effect (for details see Appendix).

polyethylene cannulae were inserted through a puncture wound into the left atrium, to be used for injection of radiolabeled microspheres and arterial blood sampling. A third catheter was inserted into the coronary sinus for venous blood sampling. Systemic blood pressure, measured through the aortic catheter with a pressure transducer, and also the ECG, were recorded continuously by strip-chart recorder. Five of the dogs were studied with C-11 PA and the other five with F-18 DG.

Tomographic imaging. The radiopharmaceuticals C-11 PA, F-18 DG, and O-15 carbon monoxide (O-15 CO) were prepared in the cyclotron and the radiopharmaceutical sections as described previously (26,27).

Positron-CT imaging was performed with a whole-body positron tomograph (28). In most instances the dogs were carefully positioned in the tomograph so that the long axis of the left ventricle was perpendicular to the imaging plane. After recording a transmission image for subsequent correction of photon attenuation, a blood-pool image was acquired for 2 min after *in vivo* labeling of red blood cells by inhalation of O-15 CO. This image was used to validate the spillover fraction from blood to myocardium (FBM) predicted by the operational

equations as discussed earlier. Fifteen minutes were allowed for physical decay of 0–15 ($T_{1/2} = 2.04$ min). Then, 5 to 25 mCi of C-11 PA or F-18 DG were administered intravenously over a 30-sec period. Serial PCT imaging was begun at the time of tracer injection. For C-11 PA, 13 2-min images were recorded over a period of about 40 min. For F-18 DG, an initial set of ten 2-min images were acquired, followed by ten 5-min images and then by ten 10-min images, resulting in a total acquisition time of ~ 3 hr. Data were acquired in the medium-resolution mode of the tomograph corresponding to an intrinsic resolution of 16 mm FWHM. The gated acquisition mode was used in order to reduce the blurring effect of cardiac motion (29). Only the diastolic portion of the cardiac cycle was selected for further data analysis. All images were corrected for physical decay of the tracer, and were normalized to the same acquisition time.

The tomograph was calibrated after each experiment with a cylindrical phantom, 20 cm in diam, that contained a solution of C-11 PA or F-18 DG. An aliquot of the solution was withdrawn with an analytical micropipette (pipetting error $< 0.8\%$) and its activity concentration determined in a well counter. From the ratio of cps per volume measured in the well counter to the cps per region-of-interest recorded from the cylinder with the tomograph, a calibration factor was derived that related tomographically measured tissue concentrations to those in the blood samples measured by well counter. All tissue and blood activity concentrations are subsequently expressed in cpm/cm^3 .

On the cross-sectional emission images, the regional myocardial and blood-pool concentrations were determined by assigning six circular regions of interest with a diameter of 8.6 mm (37 pixels) to each of the serial cross-sectional images of the myocardium. A seventh ROI was centered in the ventricular cavity in order to determine blood-pool activity. The same seven ROI matrices were also placed on the O-15 CO blood-pool image used for measurements of the spillover fraction from blood to myocardium and for validation of the predicted spillover fraction. The observed counts recorded from each ROI were then entered into a computer together with the values for the mean myocardial wall thickness and the inner diameter of the left-ventricular chamber.

Ventricular dimensions were determined postmortem as follows: At the end of each experiment, the plane of the cross-sectional image was identified on the heart with the aid of a low-power neon laser beam of the tomograph, and was carefully marked on the surface of the left ventricle. The heart was then arrested in diastole with concentrated KCl solution, then removed, and a 1-cm-thick slice of the left ventricle corresponding to the imaging plane obtained. This slice was photographed together with a metric ruler. Diastolic wall thicknesses

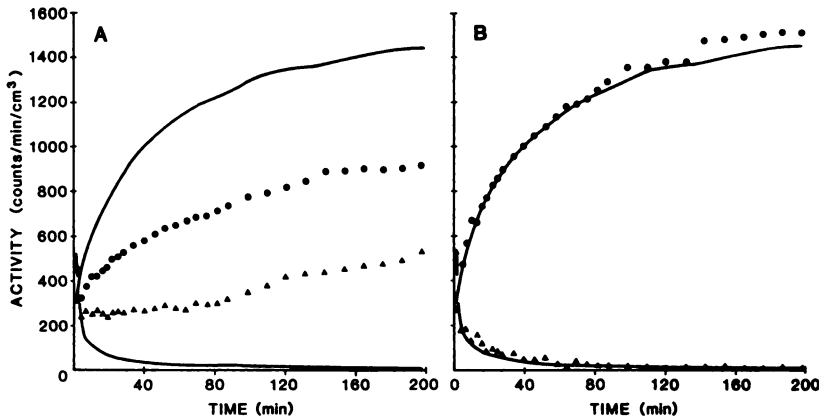


FIG. 3. Myocardial and blood-pool time-activity curves obtained from serial PCT images after intravenous F-18 deoxyglucose. Solid lines indicate true myocardial and true blood-pool activities as measured by Fick principle (myocardium) or by well counting (blood pool). Panel A plots activities observed before correction for cross-contamination and partial-volume effect; Panel B shows good agreement between myocardial and blood-pool activities measured in vivo and properly corrected, compared with true values. Note underestimation of myocardial activity before correction step, due mainly to partial-volume effect; also overestimation of blood-pool activity caused by cross-contamination from myocardial counts.

and inner diameters of the ventricle were determined for the same six ROIs as assigned on the tomograms. The mean values ($n = 6$) of wall thickness and diameter were used for data processing.

Blood sampling. In order to compare arterial activity concentrations of C-11 PA and F-18 DG measured by well counting with those determined by PCT, arterial blood sampling was performed at midpoint of each image acquisition (i.e., 1.0, 4.0, 7.0, 10.0 min). For the F-18 DG studies, additional arteriovenous blood sampling was performed to determine the myocardial tissue uptake of F-18 DG and glucose by the Fick principle. Starting at time zero, samples were withdrawn simultaneously from the left atrium and the coronary sinus every 15 sec for 3 min, and every minute for the next 12 min. The sampling interval was then progressively lengthened over the next 3 hr.

Each sample was divided into two aliquots, one for measurement of F-18 activity in whole blood, the other one immediately placed into an ice bath and centrifuged for measurement of plasma glucose concentrations. Plasma glucose levels were measured in duplicate by enzymatic techniques*.

F-18 DG activity was measured in a well counter and corrected for radioactive decay. The myocardial tissue uptake of F-18 DG was determined by integrating the arteriovenous activity differences over time, multiplied by blood flow. Myocardial time-activity curves determined in this manner were then compared with the time-activity curves measured by serial PCT. Similarly, the rate of glucose uptake was evaluated from the arteriovenous plasma concentration differences and plasma flow determined by the microsphere technique and corrected for hematocrit (Fick principle).

Measurement of myocardial blood flow. Regional myocardial blood flow was measured in duplicate with radioactive carbonized polyesterene microspheres, labeled with Co-57 or Sn-113, and the arterial reference sample technique (25). One measurement was performed before, and a second at the end of, each experiment.

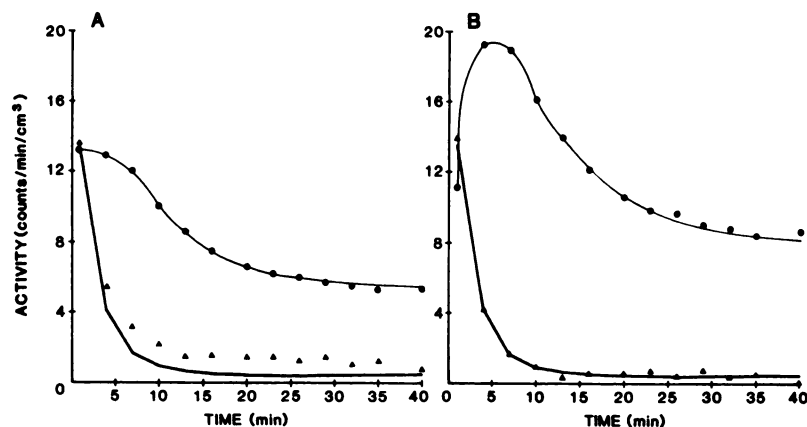
Estimation of the vascular space of myocardium.

Corrections for activity in the vascular space in myocardium (i.e., coronary arteries, capillaries, and veins) are important when true indicator tissue concentrations are to be obtained from PCT images. For example, the activity concentration derived from an ROI assigned to the LV myocardium is the sum of activity in myocardial tissue and in the vascular compartment of myocardium. To estimate the vascular space, autologous red blood cells labeled in vitro with 10 mCi of Tc-99m were injected into five dogs 5 min before sacrifice. Immediately after death, ~5 ml blood were withdrawn from the coronary sinus for well counting. The imaged slice of myocardium was divided into 20 tissue samples of ~1 g each, weighed, and the specific activity of Tc-99m measured in a well counter. The ratio of cpm/cm^3 myocardial tissue to cpm/cm^3 blood is an estimate for the fraction of blood in myocardial tissue. This fraction was relatively uniform in all five experiments, ranging from 7.9 to 11.3% with an average of $9.8 \pm 1.3\%$, and was thus similar to that reported by others (30). A constant value of 10% was therefore used in the operational equations for spillover correction.

RESULTS

Effect of correction for spillover and partial-volume effect. Typical decay-corrected time-activity curves, before and after correction for cross-contamination and partial-volume effects, are shown for F-18 DG in Fig. 3, and for C-11 PA in Fig. 4. Early after administration, F-18 DG accumulates rapidly in normal myocardium. As blood concentrations fall, the rate of accumulation declines and reaches a plateau 2–3 hr after injection. Without correction, cross-contamination early after injection leads to an overestimate of the myocardial concentrations on the initial images. Further, due to the partial-volume effect, the true activity concentration on the later parts of the time-activity curve is underestimated by about 50%, i.e., the count recovery coefficient (FMM) is about 0.5 for a wall thickness of 10 mm with

FIG. 4. Time-activity curves for myocardium and blood obtained, from serial PCT imaging after intravenous C-11 palmitate. Lower solid line indicates true blood-pool activity measured in vitro by well counting. Panel A shows blood-pool activity (\blacktriangle) from tomograms overestimated due to cross-contamination from myocardial activity, particularly on later images. Also, myocardial activity is generally underestimated mainly through partial-volume effect, although early activity is overestimated because of spillover from blood pool. Panel B shows good agreement between in vivo and in vitro measurements of blood-pool activities after deconvolution. Time course of myocardial activity now exhibits typical characteristics of C-11 palmitate kinetics in myocardium: upslope, peak activity, and subsequent down slope.



an imaging resolution of 18 mm FWHM (20). Conversely, retrieval of true blood concentrations on the very first image is relatively accurate because this image is dominated by blood activity. On the subsequent images however, blood-pool activity is markedly overestimated. After correction for cross-contamination and partial-volume effects, the blood time-activity curve determined from the tomograms approaches that determined by well counting of blood samples. Similarly, the tissue time-activity curve obtained from PCT is now virtually identical with the time-activity curve determined by the Fick principle, showing a continuous rise of activity beginning with the very first image.

The myocardial kinetics of C-11 PA are distinctively different from those of F-18 DG (Fig. 4). The corrected tissue uptake and clearance curve reveals peak activity at 4–7 min after intravenous injection. Next, an early rapid clearance phase occurs, which is nearly completed at 15–20 min after injection and is followed by a slower, late clearance phase. As with F-18 DG, myocardial activity is overestimated on the initial images when no corrections are made for cross-contamination of blood-pool activity. Conversely, the myocardial concentration in later images is underestimated by about 50%. Without correction, blood C-11 concentrations determined directly from the tomograms are accurate only on the very first image, while blood C-11 activity on the subsequent images is overestimated because of spillover of radioactivity from myocardium. Although this effect is not as pronounced as that seen with F-18 DG blood activity retrieved from the PCT images, it still leads to a significant overestimation of the arterial input function on the later time-activity curve. Correction for cross-contamination of counts and partial-volume effect resulted in accurate measurements of blood-pool activity from the PCT images, as shown by the virtually identical blood activity curves in panel B of Fig. 4.

Validation of in vivo measurements of blood and myocardial tissue activity concentrations. The accuracy of measurements of regional tracer tissue concentration by sequential tomographic imaging is illustrated in Figs. 5 and 6. For F-18 DG, the myocardial F-18 concentrations, as determined by the Fick method at different times after F-18 DG administration, are compared with the myocardial F-18 concentrations measured from the tomograms. There is good agreement between the invasive and noninvasive measurements, with a standard error of the estimate (s.e.e.) of only 363 cpm/cm³, or 4% of the mean counts. On panel B of Fig. 5, concentrations in arterial blood, withdrawn at the midpoints of acquisition and determined in a well counter as a reference, are plotted against the arterial blood-pool activity concentrations retrieved from an ROI in the center of the LV cavity on the tomographic images. Because of the wide range of data (due to the rapidly decreasing blood activity) the logarithmic values of the data are plotted. There is good agreement between the PCT and the blood F-18 concentrations determined in vitro, with an s.e.e. of only 421.5 (range from 103 to 3.1×10^9) cpm/cm³.

Comparable results were obtained for the measurements of C-11 blood concentrations after injection of C-11 PA, as shown in Fig. 6. Again, the logarithmic values were plotted. The slope of the regression line approaches unity, and the s.e.e. was only 655.8 (range from 73 to 3.1×10^9) cpm/cm³.

The validity of our correction technique is further supported by the good agreement between the blood-to-myocardium (FBM) spillover fractions measured directly after blood-pool labeling with O-15 CO, and those predicted by Eq. (A6). As listed in Table 1, the FBM measured with O-15 CO averaged 0.31 ± 0.06 , as compared with the calculated FBM of 0.29 ± 0.05 . The difference is statistically not significant. From the very

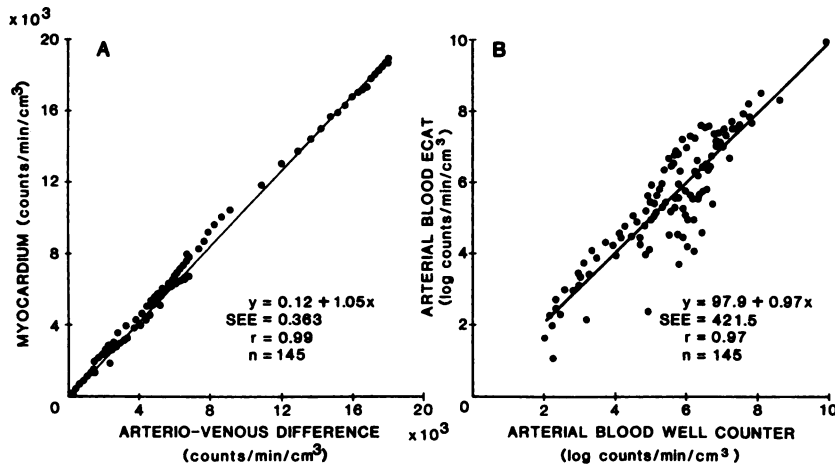


FIG. 5. Correlation between PCT myocardial (A) and PCT blood-pool (B) activities, and in vitro measurements of F-18 2-deoxyglucose. Note double-log plotting in B because of wide range of arterial blood-pool activity. Curves indicate accuracy of quantitative PCT retrieval of activity concentrations, given proper corrections for count crossover and partial-volume effects.

last image for both F-18 DG and C-11 PA, a spillover fraction from myocardium to blood (FMB) was calculated assuming that blood activities were negligible at that time, i.e., 40 min after C-11 PA and nearly 3 hr after F-18 DG administration. The measured spillover fractions (FMB) compared well with those predicted by Eq. (A2). Again, as listed in Table 1, there was no significant difference between the two kinds of measurement, although the observed spillover fractions are slightly higher than the calculated ones. This is due to the small amount of activity (1–5% of maximum activity) remaining in blood.

DISCUSSION

The results indicate that tissue concentrations of positron-emitting tracers in the heart can be measured noninvasively with PCT despite the limitations imposed by the relatively low spatial resolution of current imaging

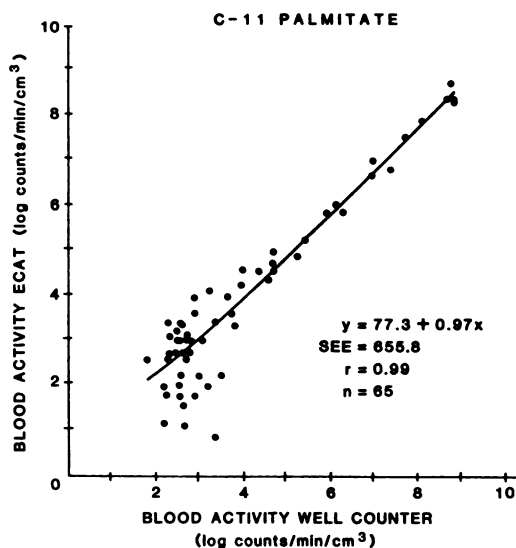


FIG. 6. Correlation between in vivo (PCT) and in vitro measurements of blood-pool activity after injection of C-11 palmitate. Note double-log plotting.

devices. The approach described in this study can be used to determine true myocardial activity concentrations even when activity concentrations in the LV blood pool and myocardium change rapidly. Earlier studies in our laboratory have demonstrated that quantitative retrieval of myocardial tissue concentrations of Ga-68-labeled albumin microspheres is possible for accurate blood-flow measurement, provided corrections are made for recovery of lost counts related to object size (partial-volume effect) by measuring LV wall thickness (22). In these experiments, however, blood concentrations were nearly zero at the time of imaging because microspheres clear almost completely from blood. Further, serial imaging is not required to measure blood flow using the microsphere-trapping technique. For evaluation of the tissue kinetics of metabolic tracers such as C-11 PA and F-18 DG, however, serial dynamic measurements of myocardial activity concentrations are essential in dealing with regional myocardial metabolism. Also, quantification of regional myocardial metabolism requires knowledge of the arterial input function, which—as the results indicate—can be obtained noninvasively. Thus, PCT of the heart allows noninvasive and simultaneous measurements of both the time-activity curve for myocardial tissue and the arterial input function, provided deconvolution of myocardial and blood-pool activity can be accomplished.

Potentially, the same correction technique described here for PCT studies can also be used for quantitative evaluation of serial SPECT images. This may be important, for example, in studies with radioiodinated analogs of free fatty acids for evaluating myocardial metabolism. However, the quantitative capability and the uniformity of the imaging resolution of SPECT need to be carefully validated before the correction technique is used.

Validation of the method. The validity of our deconvolution method was confirmed by the excellent agreement between tissue concentrations retrieved from the tomograms and those measured in vitro. For F-18 DG,

TABLE 1. GEOMETRIC MEASUREMENTS AND CORRECTION COEFFICIENTS

Dog No.	LV-dimensions		Spillover fractions			
	Radius [cm]	Wall thickness* [cm]	FBM measured	FBM predicted	FMB measured	FMB predicted
F-18 DG						
315	1.17	1.8	0.23	0.21	0.33	0.31
317	1.3	1.2	0.39	0.31	0.28	0.22
326	1.15	1.31	0.28	0.29	0.34	0.31
336	1.4	1.8	0.20	0.21	0.20	0.18
363	1.3	1.3	0.34	0.29	0.58	0.23
C-11 PA						
299	1.05	1.2	0.33	0.31	0.35	0.37
301	1.15	1.3	0.27	0.29	0.31	0.315
307	1.4	1.0	0.33	0.35	0.17	0.18
311	1.65	1.3	0.32	0.29	0.15	0.09
328	1.2	1.0	0.41	0.35	0.24	0.27

F-18 DG = F-18 deoxyglucose, C-11 PA = C-11 palmitate, FBM = spillover fraction blood to myocardium, FMB = spillover fraction myocardium to blood.

* The values given here for wall thickness in several dogs are greater than reported in the literature. This is because of inclusion of papillary muscles as well as because in several dogs the heart was sliced in an orientation that did not correspond to the perpendicular of the long axis of the left ventricle.

the accuracy of the tomographic measurements of both myocardial and blood-pool activity could be compared directly with in vitro or invasive measurements (Fig. 5). The correlation coefficients of 0.99 and 0.97 for myocardial and blood activity, respectively, for the whole group are excellent, and indicate that the approach is fundamentally sound. The correlation coefficients in individual dog experiments ranged from 0.91 to 0.99 (five for myocardial concentrations and five for blood-pool activity and thus were satisfactory in individual experiments as well.

For C-11 PA, only the retrieval of true blood activity was validated (Fig. 6). Measuring myocardial activity invasively by the Fick method and rapid a-v blood sampling—as was done with F-18 DG—is difficult because of the high extraction fraction of about 50–60% (31), and more importantly because of (a) rapidly changing blood-activity concentrations with a fast up-slope and down-slope of arterial and venous blood activity and (b) the need for separating the C-11 activity related to CO₂ or lipids.

Metabolic constants. To demonstrate the value of our approach for data retrieval in noninvasive measurements of myocardial metabolic rates of glucose, rate constants for glucose utilization were derived solely by PCT, and in Table 2 are compared with those measured by the Fick principle. In this table, the rate constants based on PCT were derived using both the retrieved myocardial and the blood-pool time-activity curves (input function) from the tomograms. Both curves were entered into the operational equation used in our laboratory for determining rate constants for glucose metabolism (8,24,32,33). This

is different from previous studies using the F-18 DG method for heart or brain that relied upon arterial blood sampling or venous-blood collection after handwarming (24) for retrieval of the input function. In Table 2, K* indicates a rate constant that combines the rate constants for forward (k₁) and reverse (k₂) membrane transport and for phosphorylation (k₃) by:

$$K^* = k_1 k_3 / (k_2 + k_3) \quad (1)$$

It is thus an indicator for the uptake rate of F-18 DG (24,32,33). From K*, the glucose (nonradioactive) plasma concentration [Glc], and the lumped constant (LC) that relates F-18 DG to nonradioactive glucose uptake in the dog's heart (24,32,33), the metabolic rate (MR) for glucose can be calculated by:

$$MR (Glc) = K^* \times [Glc] / LC \quad (2)$$

In Table 2, a value of 0.68 was used for LC (33). The good agreement between the values of MR and those from the Fick method is encouraging and indicates that in the case of the heart, metabolic rate constants can be derived entirely nontraumatically from tissue and blood-pool tracer kinetics with this new approach and without the need for arterial blood sampling. The rate constants for glucose derived noninvasively by serial gated PCT are also comparable to those reported by Ratib et al. (33). Obviously, one cannot consider this noninvasive approach for measurements of glucose metabolism completely validated in view of the limited number of studies (n = 5). Nevertheless, the present results demonstrate that the potential of this approach is worth further study.

TABLE 2. METABOLIC RATE CONSTANTS OF GLUCOSE

Dog no.	K* (F-18 DG)	Glucose [mg/100 ml]	MR (ECAT)		MR (Fick)
				[mg/min-100 g]	
315	0.0536	90.5	7.09		11.9
317	0.256	121.2	45.6		43.9
326	0.1021	119.0	17.8		19.9
336	0.183	102.0	27.4		19.9
363	0.144	87.0	18.4		6.2
Mean	0.1477	103.9	23.2		20.4
±1 s.d.	±0.077	±15.8	±14.4	NS	±14.4

K* rate constant for F-18 deoxyglucose uptake; MR = metabolic rate, discussion see text.

No metabolic model has yet been established for measuring rate constants of C-11 PA metabolism. However, as shown in recent tomographic studies (31,34), important insights into myocardial utilization of free fatty acid can be obtained from the typically biphasic myocardial time-activity curves after intravenous C-11 PA (Fig. 4), because the early rapid washout was found to be related to C-11 CO₂ production and thus to oxidation of C-11 PA (31). To date, only tissue clearance half-times and/or fractional distributions of C-11 PA between the faster and the slower turnover pools derived from the two phases of the time-activity curves have been used for quantification (31,34). As a more definitive tracer kinetic model becomes available, there will be a need for determining the arterial input function, which can then be obtained noninvasively by serial PCT imaging, as shown in Fig. 6. This will obviate the need of arterialization of venous blood through handwarming (24), which is limited in accuracy because of the relatively high extraction of free fatty acids in tissue.

Effect of spatial resolution. As can be seen in the equations of Fig. 2, both the recovery coefficients FBB

and FMM for the partial-volume effect, as well as spillover fractions FMB and FBM, are dependent upon the intrinsic resolution of the scanner system. The spatial resolution even affects FBB and FMB exponentially to the second power. It can thus be expected that both PCT and SPECT devices with good spatial resolution (35) will reduce the effect of spillover and partial-volume effect on quantitative retrieval of regional tracer concentrations in the heart. This is illustrated in Fig. 7, where simultaneous measurements of various levels of blood and myocardial tracer activity are compared in a computer simulation study for two tomographs with different spatial resolutions. From this illustration it is obvious that quantitative retrieval of both myocardial and blood-pool activity from tracer kinetic studies will be much less affected by cross-contamination of counts and partial-volume effect given tomographs of higher spatial resolution. Such tomographs may even permit in vivo measurements of LV wall thickness and ventricular diameters, especially when images are acquired in an ECG-gated mode (29).

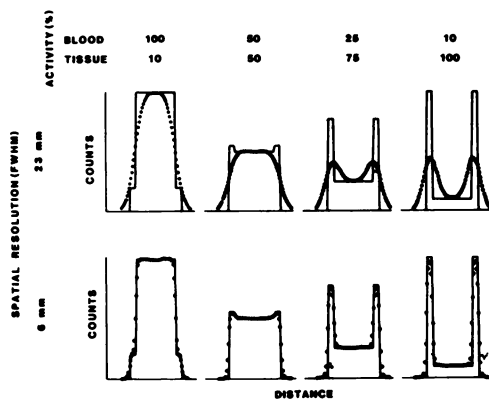


FIG. 7. Computer simulation study of phantom with different "myocardial" and "blood pool" activities. "Wall thickness" was 10 mm and "diameter" was 60 mm. Note marked improvement in retrieval of regional tracer concentrations with improved spatial resolution.

FOOTNOTE

* Autoanalyzer-glucose method.

ACKNOWLEDGMENT

Supported in part by Contract #DE-AM03-76-SF00012 between the U.S. Department of Energy, Washington, DC and the University of California at Los Angeles and The Swiss National Foundation of Research (Dr. Ratib).

APPENDIX

Derivation of equations for radioactivity spillover/corrections on cardiac cross-sectional images. By assuming an image resolution of 2.36σ FWHM (with a Gaussian point spread function) and a uniform radioactivity concentration in a circular annulus of myocardium, the imaged radioactivity at the center of the annulus can be described by:

$$\text{CMB} = \int_R^{R+d} \frac{A}{2\pi s^2} e^{-r^2/2s^2} 2\pi r dr \quad (\text{A1})$$

where A is the uniform concentration in myocardium, d is the thickness of myocardium, R is the radius of the inner circle, r is the integration parameter, and s is the spatial resolution of the system. The equation is a result of the convolution of the imaging point spread function with the distribution configuration. The integration in Eq. (A1) can be carried out and the imaged concentration CMB as a fraction of A can be expressed as:

$$FMB = \frac{CMB}{A} = e^{-R^2/2s^2} - e^{-(R+d)^2/2s^2} \quad (A2)$$

where FMB represents the crossover fraction of counts from myocardium to center of blood pool.

Also, the imaged concentration on myocardium (i.e., on the circle of radius $R + d/2$) can be approximated as equal to the case of a long straight bar of thickness d (20,22). That is, the imaged concentrations as a fraction of its true concentrations can be expressed as:

$$FMM = \frac{CMM}{A} = \int_{-d/2}^{d/2} \frac{1}{\sqrt{2\pi}s} e^{-x^2/2s^2} dx \quad (A3)$$

$$= \operatorname{erf}\left(\frac{d/2}{\sqrt{2}s}\right),$$

where erf denotes the error function (36) and FMM denotes the recovery coefficient of the myocardium concentration in image.

If the concentration in the inner circle (blood pool) is A and there is no activity in myocardium, the imaged concentration at center of blood pool relative to A is:

$$FBB = \frac{CBB}{A} = \int_0^R \frac{1}{2\pi s^2} e^{-r^2/2s^2} 2\pi r dr \quad (A4)$$

$$= 1 - e^{-R^2/2s^2}$$

This is the recovery coefficient for radioactivity in the blood pool.

The imaged concentration on myocardium (at a radius of $R + d/2$) can be approximated as equal to the concentration at a distance of $d/2$ from a large distribution of concentration A. That is, it can be approximated as:

$$CBM = \int_{d/2}^{\infty} \frac{A}{\sqrt{2\pi}s} e^{-x^2/2s^2} dx \quad (A5)$$

$$= A \cdot 0.5 \left(1 - \operatorname{erf}\left(\frac{d/2}{\sqrt{2}s}\right) \right)$$

The approximation is valid for $R \gg d$ or s , as is generally the case. For small values of R, the above approximation overestimates the true value and adjustments may be needed.

Usually, due to the vascular space in myocardium (about 10%), the contribution of blood radioactivity (A) to myocardium will be 0.1A for zero imaging spillover from the blood pool. Including this contribution, the fractional spillover from blood to myocardium on images will be:

$$FBM = CBM/A = 0.6 - 0.5 \operatorname{erf}\left(\frac{d/2}{\sqrt{2}s}\right) \quad (A6)$$

When there are radioactivities in both myocardial tissue and in blood pool, the imaged concentrations on myocardium (CMO) and in blood pool (CBO) are related to the true concentrations in myocardium (CM) and in blood (CB), as:

$$\begin{aligned} CMO &= FMM \times CM + FBM \times CB \\ CBO &= FMB \times CM + FBB \times CB \end{aligned} \quad (A7)$$

where FMM, FMB, and FBB are dependent only on the imaging resolution and the geometric configuration of the heart cross-sections, as shown earlier. Thus, CM and CB can be solved in terms of the imaged values CMO and CBO as:

$$\begin{aligned} CM &= K(FBB \times CMO - FBM \times CBO) \\ CB &= K(FMM \times CBO - FMB \times CMO) \end{aligned} \quad (A8)$$

where $K = 1/(FBB \times FMM - FMB \times FBM)$.

REFERENCES

1. PHELPS ME: Emission computed tomography. *Semin Nucl Med* 7:337-365, 1977
2. TER-POGOSSIAN MM: Basic principles of computed axial tomography. *Semin Nucl Med* 7:109-128, 1977
3. GOODWIN PN: Recent developments in instrumentation for emission computed tomography. *Semin Nucl Med* 10:322-334, 1980
4. SCHELBERT HR, HENZE E, PHELPS ME: Emission tomography of the heart. *Semin Nucl Med* 10:355-373, 1980
5. WOLF AP: Special characteristics and potential for radio-pharmaceuticals for positron emission tomography. *Semin Nucl Med* 11:2-12, 1981
6. WEISS ES, HOFFMAN EJ, PHELPS ME, et al: External detection and visualization of myocardial ischemia with ^{11}C -substrates in vitro and in vivo. *Circ Res* 39:24-32, 1976
7. LIVNI E, ELMALEH DR, LEVY S, et al: Beta-methyl[1- ^{11}C]-heptadecanoic acid: A new myocardial metabolic tracer for positron emission tomography. *J Nucl Med* 23:169-175, 1982
8. PHELPS ME, HOFFMAN EJ, SELIN C, et al: Investigation of [^{18}F]-fluoro-2-deoxyglucose for the measure of myocardial glucose metabolism. *J Nucl Med* 19:1311-1319, 1978
9. VYSKA K, FREUNDLIEB C, HOCK A, et al: The assessment of glucose transport across the blood brain barrier in man by use of 3-(^{11}C)-methyl-D-glucose. *J Cereb Flow Metab Suppl* 1:S42-S43, 1981
10. REIVICH M, KUHL D, WOLF A, et al: The (^{18}F) fluoro-deoxyglucose method for the measurement of local cerebral glucose utilization in man. *Circ Res* 44:127-137, 1979
11. GELBARD AS, CLARKE LP, LAUGHLIN JS: Enzymatic synthesis and use of ^{13}N -labeled L-asparagine for myocardial imaging. *J Nucl Med* 15:1223-1225, 1974
12. BUDINGER TF: Amino acid uptake by the myocardium. In *Nuclear Cardiology*. Willerson T. J., Ed. Philadelphia, F. A. Davis Company, 1979, pp 59-60
13. HENZE E, SCHELBERT HR, BARRIO JR, et al: Evaluation of myocardial metabolism with N-13 and C-11-labeled amino acids and positron computed tomography. *J Nucl Med* 23: 671-681, 1982
14. MACHULLA H-J, STOCKLIN G, KUPFERNAGEL CH, et al: Comparative evaluation of fatty acids labeled with C-11, Cl-34m, Br-77, and I-123 for metabolic studies of the myocardium: Concise communication. *J Nucl Med* 19:298-302, 1978
15. POE ND, ROBINSON GD JR, MACDONALD NS: Myocardial extraction of labeled long-chain fatty acid analogs. *Proc Soc Exp Biol Med* 148:215-218, 1975
16. RESKE SN, SIMON H, MACHULLA HJ, et al: Myocardial turnover of p-(I-123 phenyl)-pentadecanoic acid (IP) in patients with CAD. *J Nucl Med* 23:P34, 1982 (abst)
17. KNAPP FF, AMBROSE DKR, CALLAHAN AP, et al: Effects of chain length and tellurium position on the myocardial uptake of Te-123m fatty acids. *J Nucl Med* 22:988-993, 1981
18. SOBEL BE, WEISS ES, WELCH MJ, et al: Detection of re-

- mote myocardial infarction in patients with positron emission transaxial tomography and intravenous ^{11}C -palmitate. *Circulation* 55:853-857, 1977
19. GELTMAN EM, BIELLO D, WELCH MJ, et al: Characterization of nontransmural myocardial infarction by positron-emission tomography. *Circulation* 65:747-755, 1982
 20. HOFFMAN EJ, HUANG S-C, PHELPS ME: Quantification in positron emission computed tomography. I. Effects of object size. *J Comput Assist Tomogr* 3:299-308, 1979
 21. HENZE E, HUANG S-C, PLUMMER D, et al: Retrieval of quantitative information from positron emission computed tomographic images for cardiac studies with C-11 palmitate. *J Nucl Med* 22:P21, 1981 (abst)
 22. WISENBERG G, SCHELBERT HR, HOFFMAN EJ, et al: In vivo quantitation of regional myocardial blood flow by positron-emission computed tomography. *Circulation* 63:1248-1258, 1981
 23. PHELPS ME, MAZZIOTTA JC, HUANG SC: Study of cerebral function with positron computed tomography. *J Cereb Blood Flow Metabol* 2:113-162, 1982
 24. PHELPS ME, HUANG SC, HOFFMAN EJ, et al: Tomographic measurement of local cerebral glucose metabolic rate in man with 2-(F-18)fluoro-2-deoxy-D-glucose: Validation of the method. *Ann Neurol* 6:371-388, 1979
 25. HEYMANN MA, PAYNE BD, HOFFMAN JIE, et al: Blood flow measurements with radionuclide-labeled particles. *Prog Cardiovasc Dis* 20:55-79, 1977
 26. BARRIO JR, MACDONALD NS, ROBINSON GD JR, et al: Remote, semiautomated production of F-18-labeled 2-deoxy-2-fluoro-D-glucose. *J Nucl Med* 22:372-375, 1981
 27. PADGETT HC, ROBINSON GD, BARRIO JR: [^{11}C]palmitic acid: Improved radiopharmaceutical preparation. *Intern J Appl Rad of Isot*, 1982: in press
 28. PHELPS ME, HOFFMAN EJ, HUANG S-C, et al: ECAT: A new emission computerized tomographic imaging system for positron emitting radiopharmaceuticals. *J Nucl Med* 19:635-647, 1978
 29. HOFFMAN EJ, PHELPS ME, WISENBERG G, et al: Electrocardiographic gating in positron emission computed tomography. *J Comp Assist Tomogr* 3:733-739, 1979
 30. FRANK JS, LANGER GA: The myocardial interstitium: Its structure and its role in ionic exchange. *J Cell Biol* 60:586-601, 1974
 31. SCHELBERT HR, HENZE E, SCHON HR, et al: C-11 palmitic acid for the noninvasive evaluation of regional myocardial fatty acid metabolism with positron computed tomography. III. In vivo demonstration of the effect of substrate availability on myocardial metabolism. *Am Heart J*, 1983 (in press)
 32. HUANG SC, PHELPS ME, HOFFMAN EJ, et al: Noninvasive determination of local cerebral metabolic rate of glucose in man. *Am J Physiol* 238:E69-E82, 1980
 33. RATIB O, PHELPS ME, HUANG S-C, et al: Positron tomography with deoxyglucose for estimating local myocardial glucose metabolism. *J Nucl Med* 23:577-586, 1982
 34. LERCH RA, AMBOS HD, BERGMANN SR, et al: Localization of viable, ischemic myocardium by positron-emission tomography with ^{11}C -palmitate. *Circulation* 64:689-699, 1981
 35. HOFFMAN EJ, PHELPS ME, HUANG SC, et al: Evaluating the performance of multiplane positron tomographs designed for brain imaging. *IEEE Trans Nucl Sci*, NS-29:469-473, 1982
 36. GAUTSCHI W: Error functions and Fresnel integrals. In *Handbook of Mathematical Functions*. Abramowitz M, Segun IA, eds. Dover Publications, NY, 1968, pp 295-330

**Southern California Chapter, SNM
and
Santa Barbara Cancer Foundation
Cardiovascular Nuclear Medicine Symposium**

December 2-4, 1983

Marriott Biltmore Hotel

Santa Barbara, California

The Southern California Chapter of the Society of Nuclear Medicine and the Santa Barbara Cancer Foundation announce a Cardiovascular Nuclear Medicine Symposium to be held December 2-4, 1983, at the Marriott Biltmore Hotel, Santa Barbara, California (guaranteed rates \$59.00 single or double effective December 1-5, 1983).

Members of the Organizing Committee for the Symposium are James McClintock, M.D., Ken Lyons, M.D., Dennis O'Grady, Alan Waxman, M.D., and Daniel Berman, M.D.

Faculty

Daniel S. Berman, M.D.	Elias H. Botvinick, M.D.
Robert N. Egbert, M.D.	Ernest V. Garcia, Ph.D.
L. Stephen Graham, Ph.D.	Kenneth P. Lyons, M.D.
Jamshid Maddahi, M.D.	Frederick Mishkin, M.D.
P.K. Shaw, M.D.	Heinrich R. Schelbert, M.D., Ph.D.
James T. McClintock, M.D.	Alan D. Waxman, M.D.

Registration fee is \$70.00, if received by November 15, 1983, \$80.00 thereafter (Includes wine and cheese reception on Friday evening and a luncheon on Saturday).

For further information contact:

Justine J. Parker
PO Box 40279
San Francisco, California 94140
Tel: (415)647-0722 or 647-1668